Spectral Function of a Bosonic Ladder in an Artificial Gauge Field

Roberta Citro, Stefania de Palo, Nicolas Victorin, Anna Minguzzi, Edmond Orignac

MDPI

Article

Spectral functions of a bosonic ladder in artificial gauge field

Roberta Citro[1], Stefania De Palo[2,3], Nicolas Victorin[4], Anna Minguzzi[4], Edmond Orignac[5]

[1] Dipartimento di Fisica "E.R. Caianiello", Università degli Studi di Salerno and Unità Spin-CNR, Via Giovanni Paolo II,132, I-84084 Fisciano (Sa), Italy
[2] CNR-IOM-Democritos National Simulation Centre, UDS Via Bonomea 265, I-34136, Trieste, Italy [3] Dipartimento di Fisica Teorica, Università Trieste, Trieste, Italy [4] Univ. Grenoble-Alpes, CNRS, LPMMC, 38000 Grenoble, France [5] Univ Lyon, Ens de Lyon, Univ Claude Bernard, CNRS, Laboratoire de Physique, F-69342 Lyon, France
* Correspondence: e-mail@e-mail.com

Version November 6, 2020 submitted to Condens. Matter

Abstract: This is only the original submission, for the final version download the file from the MDPI Open Access Journal Condensed Matter. We calculate the spectral function of a boson ladder in an artificial magnetic field by means of analytic approaches based on bosonization and Bogoliubov theory. We discuss the evolution of the spectral function at increasing effective magnetic flux, from the Meissner to the Vortex phase, focussing on the effects of incommensurations in momentum space. At low flux, in the Meissner phase, the spectral function displays both a gapless branch and a gapped one, while at higher flux, in the Vortex phase, the spectral functions display two gapless branches and the spectral weight is shifted at a wavevector associated to the underlying vortex spatial structure. While the Bogoliubov theory, valid at weak interactions, predicts sharp delta-like features in the spectral function, at stronger interactions we find power-law broadening of the spectral functions due to quantum fluctuations as well as additional spectral weight at higher momenta due to backscattering and incommensuration effects. These features could be accessed in ultracold atom experiments using radio-frequency spectroscopy techniques.

Keywords: bosonization, Bogoliubov approximation, artificial gauge field, spectral functions

1. Introduction

In quasi one-dimensional systems, analogues of the Meissner and Vortex phase have been predicted for the bosonic two-leg ladder[1–4], the simplest system where orbital magnetic field effects are allowed. It was shown that in this model, the quantum phase transition between the Meissner and the Vortex phase is a commensurate-incommensurate transition[5–7]. Recently the advent of ultracold atomic gases, have opened a route where to realize low dimensional strongly interacting bosonic systems[8–10] where an artificial magnetic flux acting on the ladder can be simulated either using geometric phases[11], or the spin-orbit coupling[12,13]. Indeed, there is a mapping of the two-leg ladder bosonic model to a two-component spinor boson model in which the bosons in the upper leg become spin-up bosons and the bosons in the lower leg spin-down bosons. Under such mapping, the magnetic flux of the ladder becomes a spin-orbit coupling for the spinor bosons. Theoretical proposals to realize either artificial gauge fields and artificial spin orbit coupling have been put forward[14,15], and an artificial spin-orbit coupling has been achieved in a cold atoms experiment[16]. A two leg boson ladder under a flux is known to display a commensurate-incommensurate transition[1–4] between a low flux commensurate Meissner-like phase and a high flux incommensurate vortex-like phase. The transition has been characterized using equal time correlation functions[3,17–19]. However, we

expect a direct signature of the transition also in dynamical correlation functions. In one dimension, the low energy modes are collective excitations[20,21], and in the two-leg ladder, there is a separation between a total density ("charge") and a density difference ("spin") mode[2,4]. This is analogous to the well-known spin charge separation in electronic systems[20] and two-component boson systems[22]. Except at commensurate filling[23–26] the "charge" mode is gapless. By contrast, the "spin" mode is gapped in the Meissner phase and gapless in the Vortex phase, the transition as a function of flux being in the commensurate-incommensurate class[5,6]. Thus, the two phases are characterized by very different dynamical correlation functions. Among those correlation functions, one could for example consider the "spin-spin" dynamical structure factor. This would display a well defined gapped or gapless dispersion respectively in the Meissner and in the Vortex phase. However, such correlation function would not be sensitive to the incommensuration in the weak interchain hopping regime, although it displays incommensuration features at weak interactions and large interchain hopping[4,27]. A better indicator of incommensuration in all regimes is provided by the spectral function of the bosonic particles. In the Vortex phase, it always displays a shift in the position of the minimum of the dispersion away from $q = 0$ as a consequence of the incommensuration whereas in the Meissner state the minimum of the dispersion remains at $q = 0$. A particular feature of the single-particle spectral function is that it is incoherent[22,28] i.e. the low energy excitation branches emerge as power law singularities instead of delta function singularities. From the experimental point of view, single-particle spectral functions are accessible via radiofrequency (RF) spectroscopy techniques [29,30]. In the present paper, we calculate the boson spectral function in the different phases of the boson ladder at incommensurate filling in order to fully characterize the transition under flux.

2. Model

In the following we use the notations and definitions of Ref. [19]. We consider a model of bosons on a two-leg ladder in the presence of an artificial U(1) gauge field[13,31]:

$$H = -t\sum_{j,\sigma}(b^\dagger_{j,\sigma}e^{i\lambda\sigma}b_{j+1,\sigma} + b^\dagger_{j+1,\sigma}e^{-i\lambda\sigma}b_{j,\sigma}) + \frac{U}{2}\sum_{j,\sigma}n_{j\sigma}(n_{j\sigma}-1) + \frac{\Omega}{2}\sum_{j,\alpha,\beta}b^\dagger_{j,\alpha}(\sigma^x)_{\alpha\beta}b_{j,\beta}. \quad (1)$$

where $\sigma = \uparrow, \downarrow$ represents the leg index or the internal mode index[32–34], $b_{j,\sigma}$ annihilates a boson on leg σ on the $j-$th site, $n_{j\alpha} = b^\dagger_{j\alpha}b_{j\alpha}$, t is the hopping amplitude along the chain, Ω is the tunneling between the legs or laser induced tunneling between internal modes, λ is the flux of the effective magnetic field, U is the repulsion between bosons on the same leg. The low-energy effective theory for the Hamiltonian (1), where $\Omega \ll t$ is treated as a perturbation, is obtained by using Haldane's bosonization.[35] By introducing[35] the fields $\phi_\alpha(x)$ and $\Pi_\alpha(x)$ satisfying canonical commutation relations $[\phi_\alpha(x), \Pi_\beta(y)] = i\delta(x-y)$ as well as the dual $\theta_\alpha(x) = \pi\int^x dy\Pi_\alpha(y)$ of $\phi_\alpha(x)$, and after introducing the respective combinations of operators $\phi_{c,s} = \phi_\uparrow \pm \phi_\downarrow$ we can represent the low-energy Hamiltonian as $H = H_c + H_s$, where

$$H_c = \int \frac{dx}{2\pi}\left[u_cK_c(\pi\Pi_c)^2 + \frac{u_c}{K_c}(\partial_x\phi_c)^2\right] \quad (2)$$

describes the total density (or charge) fluctuations for incommensurate filling when umklapp terms are irrelevant, and

$$H_s = \int \frac{dx}{2\pi}\left[u_sK_s\left(\pi\Pi_s + \frac{\lambda}{a\sqrt{2}}\right)^2 + \frac{u_s}{K_s}(\partial_x\phi_s)^2\right] - 2\Omega A_0^2\int dx\cos\sqrt{2}\theta_s, \quad (3)$$

describes the antisymmetric density (or spin) fluctuations. In Eq. (2) and (3), u_s and u_c are respectively the velocity of antisymmetric and total density excitations, A_0 is a non universal coefficient[20] while K_s and K_c are the corresponding Tomonaga-Luttinger (TL) exponents[36]. For two chains of hard core bosons, we have $u_c = u_s = 2t\sin(\pi\rho^0/2)$ where ρ^0 is the average number of bosons per site and

$K_s = K_c = 1$.
The phase diagram of the Hamiltonian has been determined by looking at the behavior of the chiral current, *i.e.* the difference between the currents in upper and lower leg, which is defined as

$$J_s(j,\lambda) = -it\sum_\sigma \sigma(b^\dagger_{j,\sigma}e^{i\lambda\sigma}b_{j+1,\sigma} - b^\dagger_{j+1,\sigma}e^{-i\lambda\sigma}b_{j,\sigma}), \quad (4)$$

$$= \frac{u_s K_s}{\pi\sqrt{2}}\left(\partial_x\theta_s + \frac{\lambda}{a\sqrt{2}}\right). \quad (5)$$

As a function of the flux λ, the chiral current first increases linearly with λ while being in the Meissner phase and above a critical value of λ it starts to decrease in the Vortex phase[2]. In this phase the rung current starts to be different from zero. In Fig.1 the red-line is the phase boundary between the Vortex and the Meissner phase for the non-interacting case, while the blue-line represents the phase boundary in the hard-core limit[19]. The major difference with respect to the non-interacting case is the persistence of the Meissner phase even for large values of the flux.

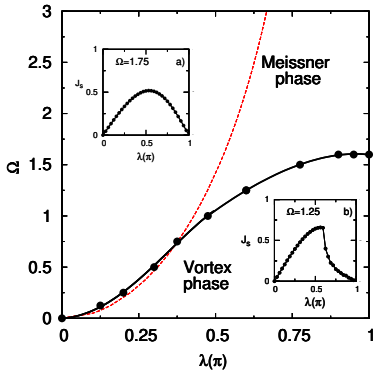

Figure 1. Phase diagram for a hard-core bosonic system on a ladder as a function of flux per plaquette λ and Ω, at the filling value $n = 1$. The black solid line that joins solid dots is the phase boundary between the Meissner and the Vortex phase, while the dashed red line is the prediction for this boundary in the non-interacting system. In the insets we show the different behavior of the spin-current $J_s(\lambda)$ for two values of interchain coupling Ω when there is the Meissner/Vortex transition and where there is not, respectively panel b) for $\Omega = 1.25$ and a) for $\Omega = 1.75$ DMRG simulation results at $L = 64$ in PBC.

Beyond the chiral and rung current the Meissner to Vortex phase transition can be traced out by looking at the behavior of the spectral function which is more sensitive to incommensurations.

For the case of lattice bosons the spectral function is defined as:

$$A_\sigma(q,\omega) = -i\sum_j \int dt\theta(t-t')e^{i(qx_j-\omega t)}\left[\langle b_{j\sigma}(t)b^\dagger_{0\sigma}(0)\rangle - \langle b^\dagger_{0\sigma}(0)b_{j\sigma}(t)\rangle\right], \quad (6)$$

and can be experimentally accessed by, e.g. via radiofrequency (RF) spectroscopy techniques [29,30]. In the following we will focus on the positive-frequency part of the spectral function, given by the first term in Eq. (6).

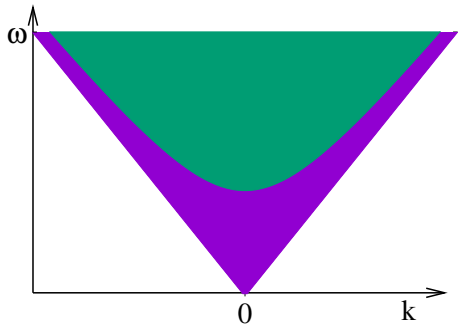

Figure 2. Schematic representation of the spectral function in the Meissner phase. The colored regions have a non-zero spectral weight. The violet region is the spectral weight coming only from the gapless charge modes, the spin modes remaining in their ground state. The green region represents the region where the gapped spin modes contribute to the spectral weight.

3. Spectral function in the Meissner phase for weak interchain hopping

Within the bosonization technique the boson annihilation operator to the lowest order approximation can be represented as:

$$\psi_\sigma(x,t) = b_{j,\sigma}(\tau)/\sqrt{a} \sim A_0 \langle e^{i\frac{\theta_s}{\sqrt{2}}} \rangle e^{i\frac{\theta_c(ja,\tau)}{\sqrt{2}}}, \tag{7}$$

where a is the lattice spacing, A_0 is a non-universal constant and σ stands for $\uparrow$ in the upper chain and $\downarrow$ for the lower chain. Knowing the Green's function for the single particle operators b one gets the spectral function as:

$$A(k,\omega) \sim A_0^2 |\langle e^{i\frac{\theta_s}{\sqrt{2}}} \rangle|^2 \int \frac{dxdt}{2\pi} e^{-i(kx-\omega t)} \left(\frac{\alpha^2}{(\alpha - iu_c t)^2 + x^2} \right)^{\frac{1}{8K_c}}, \tag{8}$$

where α is the theory cutoff taken equal to the lattice spacing. The result of the integral yields

$$A(k,\omega) \sim \frac{(A_0\alpha)^2\pi}{u_c} |\langle e^{i\frac{\theta_s(x,t)}{\sqrt{2}}} \rangle|^2 \frac{e^{2\frac{\omega}{u_c}\alpha}}{\Gamma^2\left(\frac{1}{8K_c}\right)} \left| \left(\frac{\omega^2}{u_c^2} - k^2 \right) \alpha^2 \right|^{\frac{1}{8K_c}-1} \theta(\omega)\theta\left(\frac{|\omega|}{u_c} - |k| \right), \tag{9}$$

The approximation (11) only yields the behavior of the spectral function at ω lower than the gap Δ_s in the θ_s modes. The actual correlation function can be obtained from the Form factor expansion[37–41]. The lowest contribution, from a soliton-antisoliton pair yields

$$\langle T_\tau e^{i\frac{\theta_s(x,\tau)}{\sqrt{2}}} e^{-i\frac{\theta_s(0,0)}{\sqrt{2}}} \rangle = |\langle e^{i\frac{\theta_s(x,t)}{\sqrt{2}}} \rangle|^2 + O(e^{-2\Delta_s\sqrt{(x/u_s)^2+\tau^2}}), \tag{10}$$

As a result, the Fourier transform of the full Matsubara Green's function is the sum of the contribution (9) and a second contribution analytic in a strip of the upper iv half plane of width proportional to the gap. This implies that the analytic continuation to real frequencies of this contribution is real until $\omega = 2\Delta_s$. There, a cut appears along the real frequency and the imaginary part of that contribution to the Green's function becomes nonzero. This behavior is represented schematically on Fig. 2. As the flux increases, the gap decreases linearly until it becomes zero at the commensurate-incommensurate point.

4. Spectral function in the Vortex phase for weak interchain hopping

In the vortex phase the boson field to the lowest order reads:

$$\psi_\sigma(x,t) = b_{j,\sigma}(\tau)/\sqrt{a} \sim A_0 e^{i\sigma q_0(\lambda)x_j} e^{i\frac{\theta_s(ja,\tau)}{\sqrt{2}}} e^{i\frac{\theta_c(ja,\tau)}{\sqrt{2}}}, \tag{11}$$

where $q_0(\lambda)$ is the incommensurate wavevector of the vortex phase.

Thus we find the Matsubara Green's function of the bosons in the form

$$\langle T_\tau b_{j\sigma}(\tau) b^\dagger_{0\sigma}(0)\rangle = A_0^2 e^{-i\sigma q_0(\lambda) ja} \left(\frac{a^2}{(ja)^2+(u_c\tau)^2}\right)^{\frac{1}{8K_c}} \left(\frac{a^2}{(ja)^2+(u_s\tau)^2}\right)^{\frac{1}{8K_s^*}} \tag{12}$$

and the spectral function is obtained by the integral:

$$A(k,\omega) \sim A_0^2 \int \frac{dxdt}{2\pi} e^{-i(kx-\omega t)} \left(\frac{\alpha}{\alpha - i(u_c t - x)}\right)^{\frac{1}{8K_c}} \left(\frac{\alpha}{\alpha - i(u_s t - x)}\right)^{\frac{1}{8K_s}} \left(\frac{\alpha}{\alpha - i(u_c t + x)}\right)^{\frac{1}{8K_c}} \left(\frac{\alpha}{\alpha - i(u_s t + x)}\right)^{\frac{1}{8K_s}}, \tag{13}$$

where $q_0(\lambda)$ is absorbed into k. The Fourier transform of the Matsubara Green's function (12) can be calculated by the method outlined in [22,28] and after analytic continuation $i\nu \to \omega + i0_+$ it reads:

$$G_\sigma(q,\omega) = \left(\frac{a}{2}\right)^{\frac{1}{4K_c}+\frac{1}{4K_s^*}} \frac{\Gamma\left(1-\frac{1}{8K_c}-\frac{1}{8K_s^*}\right)}{\Gamma\left(\frac{1}{8K_c}+\frac{1}{8K_s^*}\right)} |\omega^2 - u_s(q+\sigma q_0(\lambda))|^{\frac{1}{8K_c}+\frac{1}{8K_s^*}-1} e^{i\pi\left(1-\frac{1}{8K_c}-\frac{1}{8K_s^*}\right)} \Theta(\omega^2 - u_s(q+\sigma q_0(\lambda))^2)$$
$$\times \frac{1}{u_s^{\frac{1}{4K_c}+\frac{1}{4K_s^*}-1}} F_1\left(\frac{1}{8K_c}, \frac{1}{8K_c}+\frac{1}{8K_s^*}-\frac{1}{2}, 1-\frac{1}{8K_c}-\frac{1}{8K_s^*}, \frac{1}{8K_c}+\frac{1}{8K_s^*}; 1-\frac{u_c^2}{u_s^2}, 1-\frac{\omega^2-u_c^2(q+\sigma q_0(\lambda))^2}{\omega^2-u_s^2(q+\sigma q_0(\lambda))^2}\right), \tag{14}$$

where the function $F_1(a,b_1,b_2,c;z_1,z_2)$ is an Appell hypergeometric function[42], which has a series representation in terms of two complex variables z_1 and z_2 when $|z_1|<1$ and $|z_2|<1$.

Singularities appear at $\omega_1^\sigma(q,\lambda) = \pm u_c(q+\sigma q_0(\lambda))$ and at $\omega_2(q,\lambda) = \pm u_s(q+\sigma q_0(\lambda))$ and the power-law behavior of the spectral function near these points has been detailed in Ref. [28]. Some attention should be paid to extract the analytic continuation for points outside the radius of convergence of the Appell's function resorting to its integral representation possible when $\Re e[c-a] > 0$ which in our case is always true by construction: $c - a = 1/(8K_s^*)$ The behavior of the Green's function near the singularity points can be simplified as:

$$G_\sigma(q,\omega) \simeq |\omega^2 - \omega_1^\sigma(q,\lambda)^2|^{1/(8K_c)+1/(4K_s^*)-1} \tag{15}$$
$$G_\sigma(q,\omega) \simeq |\omega^2 - \omega_2^\sigma(q,\lambda)^2|^{1/(8K_s^*)+1/(4K_c)-1} \tag{16}$$

In the Vortex phase, near the commensurate-incommensurate transition the spin velocity $u_s^* \propto \sqrt{\lambda - \lambda_c}$, so we stay with the case where the charge velocity is larger than the spin one: in this case $1 - u_c^2/u_s^2 \leq 0$ and $\omega_2^\sigma(q,\lambda) \leq \omega_1^\sigma(q,\lambda)$. In this phase $K_s^* > 1/2$ and K_c is near unity, when the hopping between the chains is not too large, the imaginary part of the Greeen's function, *i.e.* the spectral function $A_\sigma(q,\omega) = -\Im m G_\sigma(q,\omega)/\pi$, is divergent near the two poles ω_1 and ω_2 as shown in panel *a*) of Fig. 3. In order to wash out at least one of the divergencies near the two poles small values of $K_c < 1/2$ are required, signalling that density wave correlations are becoming important and eventually bringing a density-wave phase. The behavior of the spin resolved spectral function $A_\sigma(q,\omega)$ for a fixed value of the applied flux is schematically shown in Fig. 4 as a function of the q and ω showing the contribution to spectral weight coming from the different singularities.

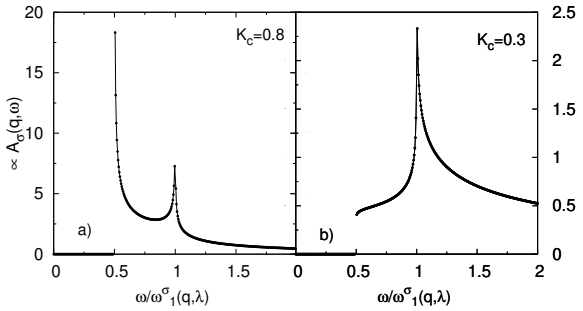

Figure 3. Spectral function $A_\sigma(q,\omega)$ as a function of $\omega/\omega_1^\sigma(q,\lambda)$ for $u_s^*/u_c = 0.5$ and $K_s^* = 0.6$. In panel a) we show the typical situation in the Vortex phase ($K_c = 0.8$) while in panel b) we show the case $K_c = 0.3$

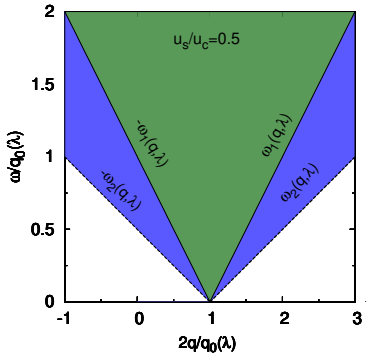

Figure 4. Schematic representation of the spectral function $A_\sigma(q,\omega)$ as a function of ω and q for a fixed applied field λ inducing a finite $q_0(\lambda)$ for $u_s^*/u_c = 0.5$. Finite spectral weights are present only in the colored region. In the blue region there is only the contribution from the singularity at $\omega_2(q,\lambda)$, while in the green one the contribution from $\omega_1(q,\lambda)$ adds up.

5. Spectral functions in the weakly interacting regime from bosonization

We adopt here an alternative bosonization scheme[4], valid at weak interactions but arbitrary inter-leg tunnel coupling Ω. In this regime, one can bosonize starting from the exact single-particle excitation spectrum [4] which displays a single minimum in the Meissner phase and two minima in the Vortex phase. In the Meissner state, the result (9) is recovered, but by construction of the bosonization scheme, the contribution of gapped modes at higher energy is not accessible.

In the Vortex phase, at low energy the field operators are approximated as [4]

$$\begin{aligned} b_{j\uparrow} &= u_Q \beta_{j+} e^{-iQj} + v_Q \beta_{j-} e^{iQj} \\ b_{j\downarrow} &= v_Q \beta_{j+} e^{-iQj} + u_Q \beta_{j-} e^{iQj} \end{aligned} \tag{17}$$

where u_Q and v_Q are the single-particle amplitudes which diagonalize the non-interacting ladder Hamiltonian, calculated at the minima $\pm Q$ of the lower branch dispersion relation, and $\beta_{j\pm} = \sum_q e^{-iqja} \beta_{q\pm Q}$ with β_k being the destruction operator of the lower single-particle excitation branch.

Then, the field operators are bosonized as $\beta_{j\pm} = \sqrt{\bar{n}} e^{i\theta_\pm(x_j)}$ and the Luttinger liquid Hamiltonian takes the usual quadratic form in the symmetric, antisymmetric sectors corresponding to the operators $\theta_{s(a)} = (\theta_+ \pm \theta_-)/\sqrt{2}$. The associated Luttinger parameters are called K_s, v_s K_a, v_a.

The Green's function, calculated *e. g.* for the upper leg $\sigma = 1/2$ reads

$$G_\uparrow(j,0) = \langle b_{j\uparrow}(t) b^\dagger_{0\uparrow}(0)\rangle = u_Q^2 \langle \beta_{j+}(t)\beta^\dagger_{0+}(0)\rangle e^{-iQj} + v_Q^2 \langle \beta_{j-}\beta^\dagger_{0-}(0) e^{iQj} \tag{18}$$

From bosonization we obtain

$$\langle \beta_{j\pm}(t)\beta^\dagger_{0\pm}(0)\rangle = \bar{n}\left(\frac{a^2}{(ja)^2 - (v_s t)^2}\right)^{1/(8K_s)} \left(\frac{a^2}{(ja)^2 - (v_a t)^2}\right)^{1/(8K_a)} \tag{19}$$

while $\langle \beta_{j\pm}(t)\beta^\dagger_{0\mp}(0)\rangle = 0$. This can be Fourier transformed as done in Sec.4, yielding a spectral function with two incoherent contributions at $q = \pm Q$, each with a power law singularity at the two excitation branches $\omega = v_{s,a}|q \pm Q|$. The same result is obtained in the lower leg, up to an exchange of u_Q^2 and v_Q^2.

6. Spectral function in the Bogoliubov theory

In the previous sections we have derived the expressions for the spectral function with the bosonization technique, valid at intermediate and strong interactions. In the regime of very weak interactions and large filling of the lattice, a complementary approach is provided by the Bogoliubov theory [27]. The system is described by a two-component Bose-Einstein condensate with wavefunction $\Psi^{(0)}_{j\sigma}$ and small fluctuations on top of it. The condensate wavefunction $\Psi^{(0)}_{j\sigma}$ is obtained by solving the coupled discrete non-linear Schroedinger equations

$$\begin{aligned}
\mu\Psi^{(0)}_{l,1} &= -t\Psi^{(0)}_{l+1,1}e^{i\lambda} - t\Psi^{(0)}_{l-1,1}e^{-i\lambda} \\
&- (\Omega/2)\Psi^{(0)}_{l,2} + U|\Psi^{(0)}_{l,1}|^2\Psi^{(0)}_{l,1} \\
\mu\Psi^{(0)}_{l,2} &= -t\Psi^{(0)}_{l+1,2}e^{-i\lambda} - t\Psi^{(0)}_{l-1,2}e^{i\lambda} \\
&- (\Omega/2)\Psi^{(0)}_{l,1} + U|\Psi^{(0)}_{l,2}|^2\Psi^{(0)}_{l,2},
\end{aligned} \tag{20}$$

where μ is the chemical potential. The field operator is approximated by

$$b_{j\sigma}(t) \simeq \Psi^{(0)}_{j\sigma} + \sum_\nu h^\sigma_{\nu j}\gamma_\nu - Q^{\sigma\,*}_{\nu j}\gamma^\dagger_\nu, \tag{21}$$

where $h^\sigma_{\nu j}$ and $Q^\sigma_{\nu j}$ are the Bogoliubov mode wavefunctions with energy ω_ν and γ_ν are the quasiparticle creation and destruction field operators, satisfying bosonic commutation relations (see [27] for the full expressions).

Using the definition (6) for the spectral function together with the mode expansion of the bosonic field operators (21) we obtain

$$A(q,\omega) = -\sum_\nu [|\tilde{h}^\sigma_{\nu q}|^2\delta(\omega - \omega_\nu) - |\tilde{Q}^\sigma_{\nu q}|^2\delta(\omega + \omega_\nu)] \tag{22}$$

where $\tilde{h}^\sigma_{\nu q} = \sum_j e^{-ikaj}h^\sigma_{\nu j}$ and $\tilde{Q}^\sigma_{\nu q} = \sum_j e^{-ikaj}Q^\sigma_{\nu j}$.

The spectral function in the Bogoliubov approximation is illustrated in Figure...

7. Conclusion

We have obtained the spectral functions of a two-leg boson ladder in an artificial gauge field. The bosonization approach, describing the regime of sufficiently strong interactions, predicts that in the Meissner phase, the low energy spectral weight is located near $\omega = 0, q = 0$. In the Vortex phase,

it is located near $\omega = 0, \pm q_0(\lambda)$. In both cases, the spectral weight is incoherent and characterized by power law singularities at $\omega = u_c|q|$ (Meissner phase) or $\omega = u_c|q \pm q_0(\lambda)|$ (Vortex phase) with known exponents, and a specific incommensuration effect due to the shift of the spectral weight for $q \simeq q_0(\lambda)$. In the Meissner phase, the gap in the antisymmetric density fluctuations translates as a power law singularity of the spectral function at frequency $\omega > 2\Delta_s$. The Bogoliubov approximation, valid at weak interactions predicts delta-like spectral function, still keeping the main features: a single gapless excitation branch and a gapped one in the Meissner phase and two gapless excitation branches displaying incommensuration effects in the Vortex phase. The Bogoliubov theory misses the backscattering contributions to the spectral function, consistently with the bosonization predictions that their spectral weight is very small at weak interactions.

The present work could be extended in different directions. Exactly at the commensurate-incommensurate transition, the antisymmetric excitations are described by a gapless theory[43] with dynamical exponent $z = 2$. The finite temperature correlation function has a known scaling form[44,45], and the spectral function at the commensurate-incommensurate transition can be obtained by convolution of that correlation function with the one of the charge modes. Such calculation is left for future work. Another possible extension is to consider the interleg interaction. Previous work has shown[36,46] that it splits the commensurate incommensurate transition point into an Ising transition point, a disorder point and a Berezinskii-Kosterltz-Thouless (BKT) transition point. An intermediate atomic density wave exists etween the Ising and the BKT point, and it develops incommensuration at the disorder point. The atomic density wave could be characterized using the spectral functions as done in the present manuscript, both in its commensurate and in its incommensurate regime. A final possible extension is to consider the spectral functions in the presence of the second incommensuration[19,47] at $\lambda = \pi n$.

1. Kardar, M. Josephson-junction ladders and quantum fluctuations. *Phys. Rev. B* **1986**, *33*, 3125.
2. Orignac, E.; Giamarchi, T. Meissner effect in a bosonic ladder. *Phys. Rev. B* **2001**, *64*, 144515.
3. Cha, M.C.; Shin, J.G. Two peaks in the momentum distribution of bosons in a weakly frustrated two-leg optical ladder. *Phys. Rev. A* **2011**, *83*, 055602.
4. Tokuno, A.; Georges, A. Ground States of a Bose-Hubbard Ladder in an Artificial Magnetic Field: Field-Theoretical Approach. *New J. Phys.* **2014**, *16*, 073005. doi:10.1088/1367-2630/16/7/073005.
5. Japaridze, G.I.; Nersesyan, A.A. *JETP Lett.* **1978**, *27*, 334.
6. Pokrovsky, V.L.; Talapov, A.L. *Phys. Rev. Lett.* **1979**, *42*, 65.
7. Schulz, H.J. *Phys. Rev. B* **1980**, *22*, 5274.
8. Jaksch, D.; Zoller, P. The cold atom Hubbard toolbox. *Ann. Phys. (N. Y.)* **2005**, *315*, 52. cond-mat/0410614.
9. Lewenstein, M.; Sanpera, A.; Ahufinger, V.; Damski, B.; Sen De, A.; Sen, U. Ultracold atomic gases in optical lattices: mimicking condensed matter physics and beyond. *Ann. Phys. (N. Y.)* **2007**, *56*, 243. cond-mat/0606771.
10. Bloch, I.; Dalibard, J.; Zwerger, W. Many-body physics with ultracold gases. *Rev. Mod. Phys.* **2008**, *80*, 885. doi:10.1103/RevModPhys.80.885.
11. Dalibard, J.; Gerbier, F.; Juzeliūnas, G.; Öhberg, P. Colloquium: Artificial gauge potentials for neutral atoms. *Rev. Mod. Phys.* **2011**, *83*, 1523.
12. Zhang, S.; Cole, W.S.; Paramekanti, A.; Trivedi, N. Spin-Orbit Coupling In Optical Lattices. In *Annual Review of Cold Atoms and Molecules*; Madison, K.W.; Bongs, K.; Carr, L.D.; Rey, A.M.; Zhai, H., Eds.; World Scientific: Singapore, 2015; Vol. 3, chapter 3, p. 135. arXiv:1411.2297, doi:10.1142/9789814667746_0003.
13. Barbarino, S.; Taddia, L.; Rossini, D.; Mazza, L.; Fazio, R. Synthetic gauge fields in synthetic dimensions: interactions and chiral edge modes. *New J. Phys.* **2016**, *18*, 035010.
14. Osterloh, K.; Baig, M.; Santos, L.; Zoller, P.; Lewenstein, M. Cold Atoms in Non-Abelian Gauge Potentials: From the Hofstadter "Moth" to Lattice Gauge Theory. *Phys. Rev. Lett.* **2005**, *95*, 010403. doi:10.1103/PhysRevLett.95.010403.

15. Ruseckas, J.; Juzeliūnas, G.; Öhberg, P.; Fleischhauer, M. Non-Abelian Gauge Potentials for Ultracold Atoms with Degenerate Dark States. *Phys. Rev. Lett.* **2005**, *95*, 010404. doi:10.1103/PhysRevLett.95.010404.
16. Lin, Y.; Jimenez-Garcia, K.; Spielman, I.B. Spin-orbit-coupled Bose-Einstein condensates. *Nature (London)* **2011**, *471*, 83.
17. Piraud, M.; Cai, Z.; McCulloch, I.P.; Schollwöck, U. Quantum magnetism of bosons with synthetic gauge fields in one-dimensional optical lattices: a Density Matrix Renormalization Group study. *Phys. Rev. A* **2014**, *89*, 063618.
18. Piraud, M.; Heidrich-Meisner, F.; McCulloch, I.P.; Greschner, S.; Vekua, T.; Schollwöck, U. Vortex and Meissner phases of strongly interacting bosons on a two-leg ladder. *Phys. Rev. B* **2015**, *91*, 140406. doi:10.1103/PhysRevB.91.140406.
19. Orignac, E.; Citro, R.; Di Dio, M.; De Palo, S.; Chiofalo, M.L. Incommensurate phases of a bosonic two-leg ladder under a flux. *New J. Phys.* **2016**, *18*, 055017. doi:10.1088/1367-2630/18/5/055017.
20. Giamarchi, T. *Quantum Physics in One Dimension*; Oxford University Press: Oxford, 2004.
21. Cazalilla, M.A.; Citro, R.; Giamarchi, T.; Orignac, E.; Rigol, M. One dimensional Bosons: From Condensed Matter Systems to Ultracold Gases. *Rev. Mod. Phys.* **2011**, *83*, 1405.
22. Kleine, A.; Kollath, C.; McCulloch, I.; Giamarchi, T.; Schollwoeck, U. Spin-charge separation in two-component Bose gases. *Phys. Rev. A* **2008**, *77*, 013607. arXiv:0706.0709.
23. Dhar, A.; Maji, M.; Mishra, T.; Pai, R.V.; Mukerjee, S.; Paramekanti, A. Bose-Hubbard model in a strong effective magnetic field: Emergence of a chiral Mott insulator ground state. *Phys. Rev. A* **2012**, *85*, 041602. doi:10.1103/PhysRevA.85.041602.
24. Dhar, A.; Mishra, T.; Maji, M.; Pai, R.V.; Mukerjee, S.; Paramekanti, A. Chiral Mott insulator with staggered loop currents in the fully frustrated Bose-Hubbard model. *Phys. Rev. B* **2013**, *87*, 174501. doi:10.1103/PhysRevB.87.174501.
25. Petrescu, A.; Le Hur, K. Bosonic Mott Insulator with Meissner Currents. *Phys. Rev. Lett.* **2013**, *111*, 150601. doi:10.1103/PhysRevLett.111.150601.
26. Petrescu, A.; Le Hur, K. Chiral Mott insulators, Meissner effect, and Laughlin states in quantum ladders. *Phys. Rev. B* **2015**, *91*, 054520. doi:10.1103/PhysRevB.91.054520.
27. Victorin, N.; Pedri, P.; Minguzzi, A. Excitation spectrum and supersolidity of a two-leg bosonic ring ladder. *Phys. Rev. A* **2020**. to appear; arXiv:1910.06410.
28. Iucci, A.; Fiete, G.A.; Giamarchi, T. Fourier transform of the $2k_F$ Luttinger liquid density correlation function with different spin and charge velocities. *Phys. Rev. B* **2007**, *75*, 205116, [arXiv:cond-mat/0702274]. doi:10.1103/PhysRevB.75.205116.
29. Dao, T.L.; Georges, A.; Dalibard, J.; Salomon, C.; Carusotto, I. Measuring the One-Particle Excitations of Ultracold Fermionic Atoms by Stimulated Raman Spectroscopy. *Phys. Rev. Lett.* **2007**, *98*, 240402. doi:10.1103/PhysRevLett.98.240402.
30. Stewart, J.T.; Gaebler, J.P.; Jin, D.S. Using photoemission spectroscopy to probe a strongly interacting Fermi gas. *Nature* **2008**, *454*, 744. doi:10.1038/nature07172.
31. Strinati, M.C.; Cornfeld, E.; Rossini, D.; Barbarino, S.; Dalmonte, M.; Fazio, R.; Sela, E.; Mazza, L. Laughlin-like states in bosonic and fermionic atomic synthetic ladders. *Phys. Rev. X* **2017**, *7*, 021033.
32. Celi, A.; Massignan, P.; Ruseckas, J.; Goldman, N.; Spielman, I.B.; Juzeliūnas, G.; Lewenstein, M. Synthetic Gauge Fields in Synthetic Dimensions. *Phys. Rev. Lett.* **2014**, *112*, 043001. doi:10.1103/PhysRevLett.112.043001.
33. Saito, T.Y.; Furukawa, S. Devil's staircases in synthetic dimensions and gauge fields. *Phys. Rev. A* **2017**, *95*, 043613.
34. Livi, L.F.; Cappellini, G.; Diem, M.; Franchi, L.; Clivati, C.; Frittelli, M.; Levi, F.; Calonico, D.; Catani, J.; Inguscio, M.; Fallani, L. Synthetic Dimensions and Spin-Orbit Coupling with an Optical Clock Transition. *Phys. Rev. Lett.* **2016**, *117*, 220401. doi:10.1103/PhysRevLett.117.220401.
35. Haldane, F.D.M. *Phys. Rev. Lett.* **1981**, *47*, 1840.
36. Citro, R.; Palo, S.D.; Dio, M.D.; Orignac, E. Quantum phase transitions of a two-leg bosonic ladder in an artificial gauge field. *Phys. Rev. B* **2018**, *97*, 174523, [arXiv:1802.04997].
37. Karowski, M.; Wiesz, P. Exact form factors in (1+1)Dimensional Field theoretic models with soliton behavior. *Nucl. Phys. B* **1978**, *139*, 455.

38. Smirnov, F.A. *Form Factors in Completely Integrable Models of Quantum Field Theory*; World Scientific: Singapore, 1992.
39. Babujian, H.; Fring, A.; Karowski, M.; Zapletal, A. Exact Form Factors in Integrable Quantum Field Theories: the Sine-Gordon Model. *Nucl. Phys. B* **1999**, *538*, 535. hep-th/9805185.
40. Babujian, H.; Karowski, M. Exact form factors in integrable quantum field theories: the sine-Gordon model (II). *Nucl. Phys. B* **2002**, *620*, 407. hep-th/0105178.
41. Essler, F.H.L.; Konik, R.M. Applications of massive integrable quantum field theories to problems in condensed matter physics. In *From Fields to Strings: Circumnavigating Theoretical Physics: Ian Kogan Memorial Collection*; Misha Shifman.; Arkady Vainshtein.; John Wheater., Eds.; World Scientific: Singapore, 2004; Vol. Part 2: From Fields to Strings – Condensed Matter, p. 684. cond-mat/0412421.
42. Olver, F.; Lozier, D.; Boisvert, R.; Clark, C., Eds. *NIST handbook of mathematical functions*; Cambridge University Press: Cambridge, UK, 2010.
43. Sachdev, S.; Senthil, T.; Shankar, R. *Phys. Rev. B* **1994**, *50*, 258.
44. Barthel, T.; Schollwöck, U.; Sachdev, S. Scaling of the thermal spectral function for quantum critical bosons in one dimension. arXiv:1212.3570, 2012.
45. Blosser, D.; Bhartiya, V.K.; Voneshen, D.J.; Zheludev, A. $z=2$ Quantum Critical Dynamics in a Spin Ladder. *Phys. Rev. Lett.* **2018**, *121*, 247201. doi:10.1103/PhysRevLett.121.247201.
46. Orignac, E.; Citro, R.; Di Dio, M.; De Palo, S. Vortex lattice melting in a boson-ladder in artificial gauge f ield. *Phys. Rev. B* **2017**, *96*, 014518. arXiv:1703.07742, doi:10.1103/PhysRevB.96.014518.
47. Di Dio, M.; De Palo, S.; Orignac, E.; Citro, R.; Chiofalo, M.L. Persisting Meissner state and incommensurate phases of hard-core boson ladders in a flux. *Phys. Rev. B* **2015**, *92*, 060506. doi:10.1103/PhysRevB.92.060506.